

# Collective emission of photons from dense, dipole-dipole interacting atomic ensembles

David Petrosyan<sup>1,2</sup> and Klaus Mølmer<sup>2</sup>

<sup>1</sup>*Institute of Electronic Structure and Laser, Foundation for Research and Technology – Hellas, GR-70013 Heraklion, Crete, Greece*

<sup>2</sup>*Department of Physics and Astronomy, Aarhus University, DK-8000 Aarhus C, Denmark*

(Dated: February 8, 2021)

We study the collective radiation properties of cold, trapped ensembles of atoms. We consider the high density regime with the mean interatomic distance being comparable to, or smaller than, the wavelength of the resonant optical radiation emitted by the atoms. We find that the emission rate of a photon from an excited atomic ensemble is strongly enhanced for an elongated cloud. We analyze collective single-excitation eigenstates of the atomic ensemble and find that the absorption/emission spectrum is broadened and shifted to lower frequencies as compared to the non-interacting (low density) or single atom spectrum. We also analyze the spatial and temporal profile of the emitted radiation. Finally, we explore how to efficiently excite the collective super-radiant states of the atomic ensemble from a long-lived storage state in order to implement matter-light interfaces for quantum computation and communication applications.

## I. INTRODUCTION

Super- and sub-radiance have been an active topic of research since the seminal paper of Dicke [1] on collective emission of atoms confined within a distance that is small compared to the wavelength of the resonantly emitted radiation. An extended atomic ensemble prepared by a laser field in the excited “timed Dicke” state collectively decays by an emission of a photon predominantly into the phase-matched direction [2, 3], while multiple scattering and reabsorption of photons in large atomic clouds modifies the exponential decay of the collective atomic excitation [3–5]. The behavior of the single excitation states of the atoms can be understood in terms of the collective eigenstates of an effective non-Hermitian Hamiltonian [6, 7] which exhibit enhanced (super-radiant) and suppressed (sub-radiant) decay rates, together with level shifts (collective Lamb shift). Recent experiments have demonstrated both sub-radiance [8, 9] and super-radiance [10–14] in large, dilute atomic clouds. In this article, we calculate the spectral and spatio-temporal properties of the emitted radiation for various trapping geometries of the atomic clouds, taking into account the interatomic interactions in the high atom density regime [15–18]. We also consider the excitation of the collective super-radiant states from a long-lived storage state of atoms for Raman conversion of an atomic spin-wave into an optical photon.

In addition to the fundamental interest in the physical processes, our study is motivated by practical applications of matter-light interfaces for quantum information processing and communications. Atomic ensembles have good coherence properties and strong dipole transitions for efficient coupling to optical photons [19–21]. Moreover, atoms can couple to microwave fields and thereby be interfaced with superconducting circuits, which are currently among the most advanced candidates for quantum processors [22]. The atomic ensembles can then play the role of quantum memories and microwave to optical transducers [22–25]. In turn, photons can serve as flying

qubits to encode and reliably transmit quantum information over long-distances [26, 27]. For optical photons, transmission may occur through free space or via fiber waveguides, and it is important to determine the spatio-temporal profile of the photon emitted by the atoms to optimally construct the paraxial optical elements that will collect the photon and direct it to a distant receiver [28].

This paper is structured as follows. In Sec. II, we present the mathematical formalism to describe the quantum interactions between  $N$  cold atoms at random positions in a trap and the quantized radiation field mediating interatomic interactions and their collective emission. In Sec. III, we discuss solutions for two-level atoms and identify how the trapping geometry influences the emission properties of the system. In Sec. IV, we extend the analysis to three-level atoms where the initial excitation is driven from a third storage state, and the excitation dynamics is influenced by the atomic interactions. Section V concludes the article and discusses the prospects of applications.

## II. QUANTUM INTERACTIONS BETWEEN ATOMS AND LIGHT

We consider  $N \gg 1$  cold atoms at random positions in a harmonic trap, with the density distribution

$$\rho(\mathbf{r}) = N \frac{\exp\left(-\frac{x^2}{2\sigma_x^2} - \frac{y^2}{2\sigma_y^2} - \frac{z^2}{2\sigma_z^2}\right)}{(2\pi)^{3/2} \sigma_x \sigma_y \sigma_z}. \quad (1)$$

The relevant internal states of the atoms are the ground state  $|g\rangle$ , an electronically excited state  $|e\rangle$ , and a long-lived storage state  $|s\rangle$ , as shown in Fig. 1.

We denote the collective ground state of the atoms as  $|G\rangle \equiv |g_1, g_2, \dots, g_N\rangle$ . A weak (single-photon) microwave or Raman process that acts symmetrically on all the atoms can transfer the ground state to the collective single-excitation storage state  $|S\rangle =$

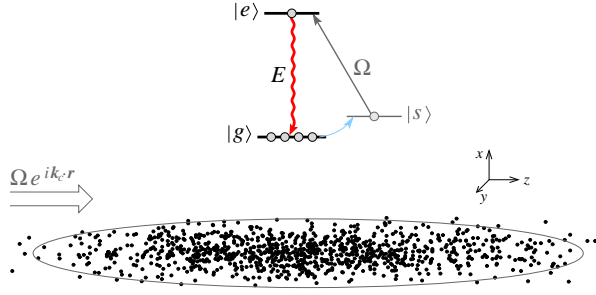


FIG. 1. Internal states and spatial configuration of an ensemble of cold atoms with random positions in an elongated harmonic trap. With all the atoms initially in the ground state  $|g\rangle$ , a weak microwave or Raman transition (light-blue arrow) creates a single collective excitation in the storage state  $|s\rangle$ . The atoms can be transferred from the storage state to the excited state  $|e\rangle$  by a laser pulse with Rabi frequency  $\Omega$  and wavevector  $\mathbf{k}_c$ . The excited state atoms decay to the ground state by emitting a photon into the free-space radiation field  $E$ .

$\frac{1}{\sqrt{N}} \sum_{j=1}^N |g_1, g_2, \dots, s_j, \dots, g_N\rangle$ . Subsequently, a spatially uniform laser pulse can near-resonantly couple the storage state  $|s\rangle$  to the excited state  $|e\rangle$  with Rabi frequency  $\Omega$ . An atom in the excited state  $|e\rangle$  can decay to the ground state  $|g\rangle$  by emitting a photon into the free-space radiation field  $\hat{\mathbf{E}}(\mathbf{r}) = \sum_k \hat{a}_k \mathbf{u}_k(\mathbf{r})$ , where  $\hat{a}_k$  are the bosonic annihilation operators for the plane-wave modes  $\mathbf{u}_k(\mathbf{r}) = \hat{\boldsymbol{\epsilon}}_{\mathbf{k},\sigma} \sqrt{\frac{\hbar\omega_k}{2\epsilon_0 V}} e^{i\mathbf{k}\cdot\mathbf{r}}$  forming a complete basis for the field within the quantization volume  $V$ . The Hamiltonian of the system is

$$H = \sum_k \hbar\omega_k \hat{a}_k^\dagger \hat{a}_k + \sum_{j=1}^N \sum_{\mu=g,s,e} \hbar\omega_\mu |\mu\rangle_j \langle \mu| - \sum_{j=1}^N [\hbar\Omega e^{i(\mathbf{k}_c \cdot \mathbf{r}_j - \omega_c t)} |e\rangle_j \langle s| + \wp_{eg} \cdot \hat{\mathbf{E}}(\mathbf{r}_j) |e\rangle_j \langle g| + \text{H.c.}], \quad (2)$$

where the first term on the r.h.s. is the Hamiltonian for the field modes with energies  $\hbar\omega_k$ , the second term corresponds to the Bohr energies  $\hbar\omega_\mu$  of the atomic levels  $|\mu\rangle$  ( $\mu = g, s, e$ ), the third term describes the interaction of the atoms at positions  $\mathbf{r}_j$  with the coupling laser with frequency  $\omega_c$  and wavevector  $\mathbf{k}_c \parallel \hat{\mathbf{z}}$ , and the last term describes the coupling of the atoms to the quantized free-space radiation field with the dipole moment  $\wp_{eg}$  on the transition  $|e\rangle \rightarrow |g\rangle$ . For simplicity, we neglect the coupling of the atoms with the free-space radiation and the resulting decay on the  $|e\rangle \rightarrow |s\rangle$  transition [29]. We set the energy of the ground state to zero,  $\hbar\omega_g = 0$ , and assume that  $\omega_s \ll \omega_e$  ( $\omega_c \simeq \omega_e$ ).

The state vector of the system with the single atomic

or photonic excitation can be expanded as

$$|\Psi\rangle = \sum_j c_j e^{-i\omega_s t} |s_j\rangle \otimes |0\rangle + \sum_j b_j e^{-i\omega_e t} |e_j\rangle \otimes |0\rangle + |G\rangle \otimes \sum_k a_k e^{-i\omega_k t} |1_k\rangle,$$

where  $|G\rangle \equiv |g_1, g_2, \dots, g_N\rangle$ ,  $|s_j\rangle \equiv |g_1, g_2, \dots, s_j, \dots, g_N\rangle$ ,  $|e_j\rangle \equiv |g_1, g_2, \dots, e_j, \dots, g_N\rangle$ , while  $|1_k\rangle \equiv \hat{a}_k^\dagger |0\rangle$  denotes the state of the radiation field with a single photon in mode  $k$ . The state vector evolves according to the Schrödinger equation  $\partial_t |\Psi\rangle = -\frac{i}{\hbar} H |\Psi\rangle$ , leading to a set of equations for the atomic amplitudes

$$\begin{aligned} \partial_t c_j &= i\Omega^* e^{-i\mathbf{k}_c \cdot \mathbf{r}_j} b_j e^{i\Delta_c t}, \\ \partial_t b_j &= i\Omega e^{i\mathbf{k}_c \cdot \mathbf{r}_j} c_j e^{-i\Delta_c t} + i \sum_k g_k(\mathbf{r}_j) a_k e^{i(\omega_e - \omega_k)t} \end{aligned} \quad (3a)$$

with  $\Delta_c = \omega_c - \omega_e$ , and an equation for the field amplitudes cast in the integral form

$$a_k(t) = i \sum_j g_k^*(\mathbf{r}_j) \int_0^t dt' b_j(t') e^{i(\omega_k - \omega_e)t'}, \quad (4)$$

where  $g_k(\mathbf{r}_j) = \frac{\wp_{eg} \cdot \mathbf{u}_k(\mathbf{r}_j)}{\hbar}$  is the atom-field coupling strength.

### A. Atoms

Let us for the moment disregard the storage state and the transition  $|s\rangle \rightarrow |e\rangle$ , assuming  $\Omega = 0$ , and consider two-level atoms with the ground  $|g\rangle$  and excited  $|e\rangle$  states. We substitute Eq. (4) into Eq. (3b) and use the Born-Markov approximation to eliminate the radiation field [15, 16], obtaining a closed set of equations for the atomic amplitudes

$$\partial_t b_j = -\frac{1}{2}\Gamma b_j - \frac{1}{2}\Gamma \sum_{i \neq j} F_{ji} b_i. \quad (5)$$

Here  $\Gamma = \frac{1}{4\pi\epsilon_0} \frac{4k_e^3 |\wp_{eg}|^2}{3\hbar}$  is the usual spontaneous decay rate of the atom in the excited state  $|e\rangle$  whose Lamb shift can be incorporated into  $\omega_e$  [33, 34], and  $F_{ji} = f_{ji} + ig_{ji}$  is the complex dipole-dipole exchange interaction (including the near-field terms) between the atoms,

$$\begin{aligned} f_{ji} &= \frac{3}{2} [1 - (\hat{\boldsymbol{\rho}} \cdot \hat{\mathbf{r}}_{ij})^2] \frac{\sin(k_e r_{ij})}{k_e r_{ij}} \\ &+ \frac{3}{2} [1 - 3(\hat{\boldsymbol{\rho}} \cdot \hat{\mathbf{r}}_{ij})^2] \left[ \frac{\cos(k_e r_{ij})}{(k_e r_{ij})^2} - \frac{\sin(k_e r_{ij})}{(k_e r_{ij})^3} \right], \\ g_{ji} &= -\frac{3}{2} [1 - (\hat{\boldsymbol{\rho}} \cdot \hat{\mathbf{r}}_{ij})^2] \frac{\cos(k_e r_{ij})}{k_e r_{ij}} \\ &+ \frac{3}{2} [1 - 3(\hat{\boldsymbol{\rho}} \cdot \hat{\mathbf{r}}_{ij})^2] \left[ \frac{\sin(k_e r_{ij})}{(k_e r_{ij})^2} + \frac{\cos(k_e r_{ij})}{(k_e r_{ij})^3} \right], \end{aligned}$$

where  $\hat{\boldsymbol{\rho}} \equiv \frac{\boldsymbol{\rho}_{eg}}{\rho_{eg}}$  is the unit vector in the direction of the atomic dipole moment,  $\hat{\mathbf{r}}_{ij} \equiv \frac{\mathbf{r}_{ij}}{r_{ij}}$  is the unit vector along the direction of the relative position vector  $\mathbf{r}_{ij} = \mathbf{r}_i - \mathbf{r}_j$  between atoms  $i$  and  $j$ ,  $r_{ij} \equiv |\mathbf{r}_{ij}|$  is the distance between the atoms, and  $k_e = \omega_e/c = 2\pi/\lambda_e$  with  $\lambda_e$  being the wavelength of the resonant photon. Note that for an isotropic dipole moment  $(\hat{\boldsymbol{\rho}} \cdot \hat{\mathbf{r}}_{ij})^2 = \frac{1}{3} \forall \hat{\mathbf{r}}_{ij}$  (or for sufficiently low density with the mean interatomic separation  $\langle r_{ij} \rangle > \lambda_e$ ) the interatomic interaction takes the simple form  $F_{ji} = \frac{e^{ik_e r_{ij}}}{ik_e r_{ij}}$  (or  $F_{ji} \simeq \frac{3}{2} [1 - (\hat{\boldsymbol{\rho}} \cdot \hat{\mathbf{r}}_{ij})^2] \frac{e^{ik_e r_{ij}}}{ik_e r_{ij}}$ ) [5, 7].

## B. Radiation Field

Consider now the wavefunction [32, 33] of the emitted single-photon field

$$\begin{aligned} \mathbf{E}(\mathbf{r}, t) &\equiv \langle 0 | \langle G | \hat{\mathbf{E}}(\mathbf{r}) | \Psi(t) \rangle = \sum_{\mathbf{k}} \mathbf{u}_{\mathbf{k}}(\mathbf{r}) a_{\mathbf{k}}(t) e^{-i\omega_{\mathbf{k}} t} \\ &= i \frac{\wp_{eg}}{2\epsilon_0 V} \sum_{\mathbf{k}, \sigma} \hat{\boldsymbol{\epsilon}}_{\mathbf{k}, \sigma} (\hat{\boldsymbol{\rho}} \cdot \hat{\boldsymbol{\epsilon}}_{\mathbf{k}, \sigma}) \omega_{\mathbf{k}} \sum_j e^{i\mathbf{k} \cdot (\mathbf{r} - \mathbf{r}_j)} \\ &\quad \times \int_0^t dt' b_j(t') e^{-i\omega_{\mathbf{k}}(t-t') - i\omega_e t'}. \end{aligned} \quad (6)$$

We sum over the two orthogonal photon polarizations  $\sigma = 1, 2$  for each  $\mathbf{k}$  ( $\hat{\boldsymbol{\epsilon}}_{\mathbf{k}, \sigma} \perp \mathbf{k}$ ),  $\sum_{\sigma} \hat{\boldsymbol{\epsilon}}_{\mathbf{k}, \sigma} \cdot \hat{\boldsymbol{\epsilon}}_{\mathbf{k}, \sigma} = \mathbb{I} - \hat{\mathbf{k}} \otimes \hat{\mathbf{k}}$ , where  $\mathbb{I}$  is the unity tensor and  $\hat{\mathbf{k}} \equiv \frac{\mathbf{k}}{k}$ , and replace the summation over the modes  $\mathbf{k}$  by an integration via  $\sum_{\mathbf{k}} \rightarrow \frac{V}{(2\pi)^3} \int d^3 k = \frac{V}{(2\pi)^3} \int_0^\infty dk k^2 \int_{4\pi} d\Omega_k$  [33, 34], obtaining

$$\begin{aligned} \mathbf{E}(\mathbf{r}, t) &= i \frac{\wp_{eg}}{2(2\pi)^3 \epsilon_0} \sum_j \int_0^t dt' b_j(t') e^{-i\omega_e t'} \\ &\quad \times \int_0^\infty dk k^2 \omega_k e^{-i\omega_k(t-t')} \\ &\quad \times \int_{4\pi} d\Omega_k e^{i\mathbf{k} \cdot (\mathbf{r} - \mathbf{r}_j)} [\mathbb{I} - \hat{\mathbf{k}} \otimes \hat{\mathbf{k}}] \cdot \hat{\boldsymbol{\rho}}, \end{aligned} \quad (7)$$

The integration over the  $4\pi$  solid angle with  $d\Omega_k = \sin\theta d\theta d\varphi$  leads to  $4\pi \frac{\sin(k|\mathbf{r} - \mathbf{r}_j|)}{k|\mathbf{r} - \mathbf{r}_j|} [\mathbb{I} - \hat{\mathbf{r}}_j \otimes \hat{\mathbf{r}}_j] = -i \frac{2\pi c [\mathbb{I} - \hat{\mathbf{r}}_j \otimes \hat{\mathbf{r}}_j]}{\omega_k |\mathbf{r} - \mathbf{r}_j|} (e^{ik|\mathbf{r} - \mathbf{r}_j|} - \text{c.c.})$ , where  $\hat{\mathbf{r}}_j \equiv \frac{\mathbf{r}_j}{r_j}$ . We substitute this into the above equation, assume that during the photon emission  $k$  is peaked around the atomic resonance  $k_e = \omega_e/c$  and pull  $k_e^2$  out of the integral, and extend the lower limit of integration over  $k$  to  $-\infty$ , as in the Weisskopf-Wigner approximation [32, 33]. We then have

$$\begin{aligned} &\int_{-\infty}^\infty dk (e^{ik|\mathbf{r} - \mathbf{r}_j| - ick(t-t')} - e^{-ik|\mathbf{r} - \mathbf{r}_j| - ick(t-t')}) \\ &= \frac{2\pi}{c} \delta(t' - t + |\mathbf{r} - \mathbf{r}_j|/c) + \frac{2\pi}{c} \delta(t' - t - |\mathbf{r} - \mathbf{r}_j|/c). \end{aligned}$$

Upon substitution into Eq. (7) the second term is always zero, and we finally obtain

$$\begin{aligned} \mathbf{E}(\mathbf{r}, t) &= \frac{\wp_{eg} k_e^2}{4\pi\epsilon_0} \sum_j \frac{e^{-i\omega_e(t - |\mathbf{r} - \mathbf{r}_j|/c)}}{|\mathbf{r} - \mathbf{r}_j|} b_j(t - |\mathbf{r} - \mathbf{r}_j|/c) \\ &\quad \times [\mathbb{I} - \hat{\mathbf{r}}_j \otimes \hat{\mathbf{r}}_j] \cdot \hat{\boldsymbol{\rho}}. \end{aligned} \quad (8)$$

For a single atom at the origin, we have a (in general anisotropic) spherical wave  $\mathbf{E}(\mathbf{r}, t) = \frac{\wp_{eg} k_e^2 e^{-i\omega_e(t-r/c)}}{4\pi\epsilon_0 r} b(t-r/c) [\mathbb{I} - \hat{\mathbf{r}}_j \otimes \hat{\mathbf{r}}_j] \cdot \hat{\boldsymbol{\rho}}$ , while the intensity of the emitted radiation in the direction of  $\mathbf{r}$  is  $I_\sigma(\mathbf{r}, t) = \frac{\epsilon_0 c}{2} |\hat{\boldsymbol{\epsilon}}_{\mathbf{r}, \sigma} \cdot \mathbf{E}(\mathbf{r}, t)|^2 = \frac{\hbar\omega_e}{4\pi r^2} \frac{3|\hat{\boldsymbol{\epsilon}}_{\mathbf{r}, \sigma} \cdot \hat{\boldsymbol{\rho}}|^2}{8} \Gamma |b(t-r/c)|^2$  for each polarization component  $\hat{\boldsymbol{\epsilon}}_{\mathbf{r}, \sigma} \perp \mathbf{r}$ . As an example, for  $\Delta M = \pm 1$  atomic transition with  $\hat{\boldsymbol{\rho}} = \frac{1}{\sqrt{2}}(\hat{\mathbf{x}} \pm i\hat{\mathbf{y}})$  we obtain the dipole emission pattern  $I_1 + I_2 \propto \frac{1}{2}(1 + \cos^2\theta)$ .

In the far-field region, we have  $|\mathbf{r} - \mathbf{r}_j| \simeq r - (\mathbf{r} \cdot \mathbf{r}_j)/r = r - \hat{\mathbf{r}} \cdot \mathbf{r}_j$ , and therefore

$$\mathbf{E}_\sigma^{(\text{ff})}(\mathbf{r}, t) = (\hat{\boldsymbol{\epsilon}}_{\mathbf{r}, \sigma} \cdot \hat{\boldsymbol{\rho}}) \frac{\wp_{eg} k_e^2}{4\pi\epsilon_0} \frac{e^{i(k_e r - \omega_e t)}}{r} \sum_j b_j(t-r/c) e^{-i\mathbf{k}_e \cdot \mathbf{r}_j}, \quad (9)$$

where  $\mathbf{k}_e \equiv k_e \hat{\mathbf{r}}$ .

### Non-interacting atoms

Consider an ensemble of  $N$  atoms with density  $\rho(\mathbf{r})$ , such that  $\int d^3 r \rho(\mathbf{r}) = N$ , prepared initially in the collective single-excitation (timed-Dicke [2]) state  $|E_{\text{TD}}\rangle = \frac{1}{\sqrt{N}} \sum_{j=1}^N e^{i\mathbf{k}_c \cdot \mathbf{r}_j} |e_j\rangle$ . For non-interacting atoms,  $F_{ji} = 0$ , we have from Eq. (5) that  $b_j(t) = \frac{1}{\sqrt{N}} e^{-\frac{1}{2}\Gamma t} e^{i\mathbf{k}_c \cdot \mathbf{r}_j}$ . Disregarding the photon polarization, the emitted field in the far-field region is

$$\mathbf{E}^{(\text{ff})}(\mathbf{r}, t) = \frac{\wp_{eg} k_e^2}{4\pi\epsilon_0} \frac{e^{-\frac{1}{2}\Gamma(t-r/c)}}{\sqrt{N}} e^{-i\omega_e t} \mathcal{E}(\mathbf{r}), \quad (10a)$$

$$\begin{aligned} \mathcal{E}(\mathbf{r}) &\equiv \frac{e^{i\mathbf{k}_e \cdot \mathbf{r}}}{r} \sum_j e^{i(\mathbf{k}_c - \mathbf{k}_e) \cdot \mathbf{r}_j} \\ &= \frac{e^{i\mathbf{k}_e \cdot \mathbf{r}}}{r} \int d^3 r' \rho(\mathbf{r}') e^{i(\mathbf{k}_c - \mathbf{k}_e) \cdot \mathbf{r}'}. \end{aligned} \quad (10b)$$

Substituting here the Gaussian density distribution  $\rho(\mathbf{r}')$  of Eq. (1) and performing the integration over  $\mathbf{r}'$ , we obtain

$$\mathcal{E}(\mathbf{r}) = N \frac{e^{i\mathbf{k}_e \cdot \mathbf{r}}}{r} \exp \left\{ -\frac{k_e^2}{2} \left[ \frac{x^2 + y^2}{r^2} \sigma_\perp^2 + \frac{(z-r)^2}{r^2} \sigma_z^2 \right] \right\}, \quad (11)$$

where we assume that  $\sigma_{x,y} = \sigma_\perp$ . Consider the field amplitude  $\mathcal{E}(\mathbf{r})$  along the  $z$  direction within a small axial distance  $\varrho = \sqrt{x^2 + y^2} \ll z$ , such that  $r = \sqrt{z^2 + \varrho^2} \simeq z + \frac{\varrho^2}{2z}$ . With  $r^2 \approx z^2$  and  $(r-z)^2 \approx 0$ , we have from Eq. (11)

$$\mathcal{E}(\mathbf{r}) \approx \frac{N}{z + \frac{\varrho^2}{2z}} \exp \left[ ik_e \left( z + \frac{\varrho^2}{2z} \right) - \frac{k_e^2}{2} \frac{\varrho^2}{z^2} \sigma_\perp^2 \right]. \quad (12)$$

On the other hand, a Gaussian field mode with the waist  $w_0$  at  $z = 0$  has the form

$$\phi_k(\mathbf{r}) = \frac{\zeta_k}{q_k^*(z)} \exp \left[ ik \left( z + \frac{\varrho^2}{2q_k^*(z)} \right) \right], \quad (13)$$

where  $\zeta_k = kw_0^2/2$  is the Rayleigh length and  $q_k(z) = z + i\zeta_k$  is the complex beam parameter. In the far field,  $z^2 + \zeta_k^2 \approx z^2$ , we have

$$\phi_k(\mathbf{r}) \approx \frac{\zeta_k}{z - i\zeta_k} \exp \left[ ik \left( z + \frac{\varrho^2}{2z} \right) - \frac{k^2 \varrho^2 \zeta_k}{2 z^2 k} \right]. \quad (14)$$

Comparing this with Eq. (12), we see that, apart from the Gouy phase that originates from the imaginary part of  $\frac{\zeta_k}{z - i\zeta_k}$ , the far field  $\mathcal{E}(\mathbf{r})$  is mostly emitted into a Gaussian mode with wavevector  $k = k_e$  and a beam waist determined from  $\zeta_k/k = w_0^2/2 \approx \sigma_\perp^2$ , i.e.,  $w_0 = \sqrt{2}\sigma_\perp$ , while the angular spread (divergence) of the beam is  $\Delta\theta = \frac{\lambda_e}{\pi w_0} = \frac{\sqrt{2}}{k_e \sigma_\perp}$ . More qualitatively [30, 31], the probability of the cooperative photon emission into the phase-matched direction within the solid angle  $\Delta\Omega = \pi(\Delta\theta)^2 = \frac{2\pi}{(k_e \sigma_\perp)^2}$ , as opposed to spontaneous, uncorrelated photon emission into the  $4\pi$  solid angle, is

$$P_{\Delta\Omega} \simeq \frac{N\Delta\Omega}{4\pi + N\Delta\Omega}. \quad (15)$$

### III. TWO-LEVEL ATOMIC MEDIUM

#### A. Collective decay dynamics of interacting atoms

Let us assume that at some initial time  $t = 0$  the atoms are prepared by a laser in the collective single-excitation (timed-Dicke [2]) state

$$|E_{\text{TD}}\rangle = \frac{1}{\sqrt{N}} \sum_{j=1}^N e^{i\mathbf{k}_c \cdot \mathbf{r}_j} |e_j\rangle = \frac{1}{\sqrt{N}} \sum_{j=1}^N |\tilde{e}_j\rangle, \quad (16)$$

with  $|\tilde{e}_j\rangle \equiv e^{i\mathbf{k}_c \cdot \mathbf{r}_j} |e_j\rangle$  and  $\mathbf{k}_c \parallel \hat{z}$ . We expand the state of the atomic ensemble as  $|\Psi\rangle = \sum_j b_j e^{-i\omega_e t} |e_j\rangle \equiv \sum_j \tilde{b}_j e^{-i\omega_e t} |\tilde{e}_j\rangle$ , where the slowly varying in time and space excited state amplitudes  $\tilde{b}_j = e^{-i\mathbf{k}_c \cdot \mathbf{r}_j} b_j$  obey the equations

$$\partial_t \tilde{b}_j = -\frac{1}{2}\Gamma \tilde{b}_j - \frac{1}{2}\Gamma \sum_{i \neq j} F_{ji} e^{i\mathbf{k}_c \cdot \mathbf{r}_{ij}} \tilde{b}_i \quad (17)$$

with the initial conditions  $\tilde{b}_j(0) = \frac{1}{\sqrt{N}} \forall j$ . For a non-interacting atomic ensemble,  $F_{ji} \rightarrow 0$ , i.e., in the dilute regime of large mean interatomic separation  $\langle r_{ij} \rangle \gtrsim N^{1/4}(\sigma_z \lambda_e)^{1/2}$ , the initial state  $|\Psi(0)\rangle = |E_{\text{TD}}\rangle$  will decay with the single-atom rate  $\Gamma$  to the collective ground state  $|G\rangle$  and emit a photon with the spatial profile of Eq. (12). But in the high-density regime, the interatomic

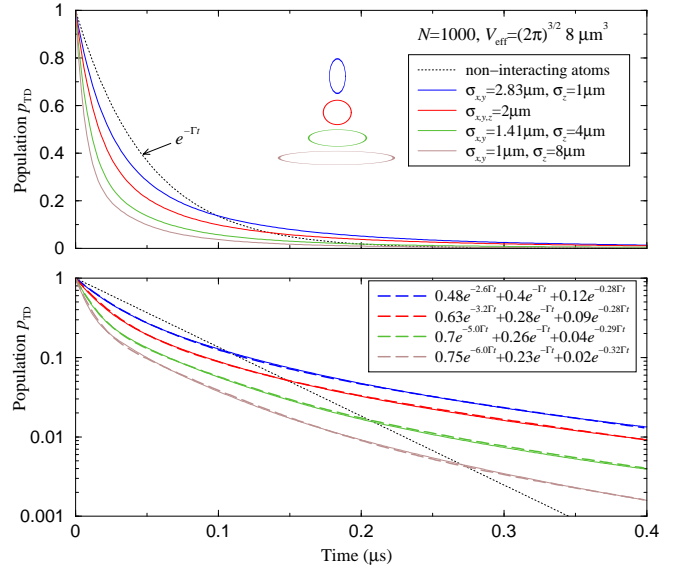


FIG. 2. Dynamics of the population  $p_{\text{TD}}(t) = |\langle E_{\text{TD}} | \Psi(t) \rangle|^2$  of the initially prepared timed-Dicke state  $|E_{\text{TD}}\rangle$  of the atoms in a harmonic trap with different aspect ratios  $\sigma_{x,y}/\sigma_z$ ; The progressively lower curves correspond to decreasing  $\sigma_{x,y}$  and increasing  $\sigma_z$ , with the product  $\sigma_x \sigma_y \sigma_z$  kept constant. We place  $N = 1000$  atoms at random positions in an effective volume  $V_{\text{eff}} = (2\pi)^{3/2} \sigma_x \sigma_y \sigma_z = (2\pi)^{3/2} 8 \mu\text{m}^3$ , i.e., the mean interatomic separation  $\langle r_{ij} \rangle = \sqrt[3]{V_{\text{eff}}/N} \simeq 0.5 \mu\text{m}$ . Each curve corresponds to a single realization of the ensemble of atoms at random positions, but different realizations for the same atom number and trap geometry give very similar results (for large enough  $N$  as here). The wavelength of the resonant transition  $|e\rangle \rightarrow |g\rangle$  is  $\lambda_e = 780 \text{ nm}$ , decay rate  $\Gamma = 2 \times 10^7 \text{ s}^{-1}$ , and the transition dipole moment is along  $\hat{\phi} = \frac{\hat{x} + i\hat{y}}{\sqrt{2}}$  ( $\Delta M = 1$  transition). In the lower panel, we fit the population decay curves with the sum of three exponential terms,  $p_{\text{TD}}(t) \simeq p_1 e^{-\Gamma_S t} + p_2 e^{-\Gamma t} + p_3 e^{-\Gamma_S t}$ , having super-radiant  $\Gamma_S > \Gamma$ , single-atom  $\Gamma$ , and sub-radiant  $\Gamma_S < \Gamma$  decay rates.

dipole-dipole interaction mediated by the multiple scattering of the photon by the atoms, significantly modifies this behavior, resulting in both accelerated (super-radiant) decay with rate  $\Gamma_S > \Gamma$  and decelerated (sub-radiant) decay with the rate  $\Gamma_S < \Gamma$ , as seen in Fig. 2. Moreover, for a fixed mean density of the atom cloud, the super- and sub-radiant decays strongly depend on the geometry of the atom cloud: atoms in an elongated trap,  $\sigma_z > \sigma_{x,y}$ , typically decay faster, which can be attributed to the constructive interference of the photon emission (scattering) in the forward direction with larger optical depth. We can approximate the super-radiant decay rate as

$$\Gamma_S \approx \mathcal{G} \frac{N}{k_e^2 \sigma_{x,y}^2} \Gamma, \quad (18)$$

where the numerical factor  $\mathcal{G}$  depends on the geometry of the atom cloud ( $\mathcal{G} \approx \frac{4}{3}, \frac{5}{6}, \frac{2}{3}, \frac{2}{5}$  for the four geometries shown in Figs. 2, 3). This is consistent with

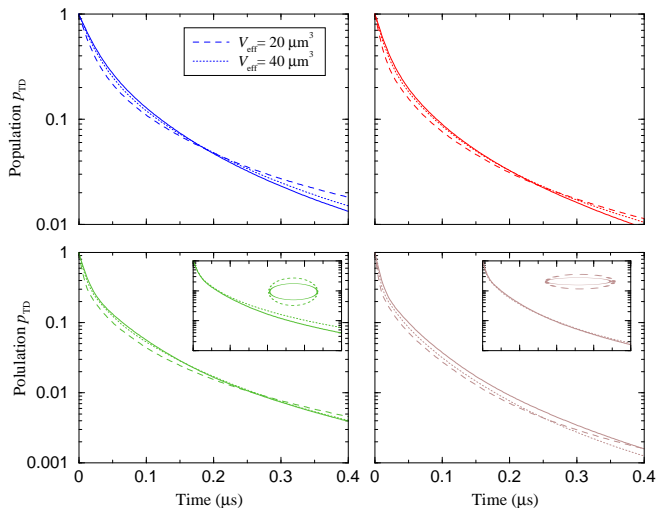


FIG. 3. Same as in Fig. 2 (thin solid lines are for reference, with the upper-left, upper-right, lower-left and lower-right panels corresponding to decreasing  $\sigma_{x,y}$  and increasing  $\sigma_z$ ), but for  $N = 2000$  atoms, in traps with the same volume  $V_{\text{eff}} = (2\pi)^{3/2}8\mu\text{m}^3$  but twice the atom density (dashed lines), or in traps with rescaled dimensions  $\sigma_{x,y,z} \rightarrow \sqrt[3]{2}\sigma_{x,y,z}$  and twice the volume  $V_{\text{eff}} = (2\pi)^{3/2}16\mu\text{m}^3$  but the same density as in Fig. 2 (dotted lines). The insets in the lower panels show the decay dynamics for  $N = 2000$  atoms in the elongated traps with the same lengths  $\sigma_z = 4, 8\mu\text{m}$  but larger widths  $\sigma_{x,y} \rightarrow \sqrt{2}\sigma_{x,y}$  and twice the volume  $V_{\text{eff}} = (2\pi)^{3/2}16\mu\text{m}^3$ , i.e. the same density as in Fig. 2.

the previously derived results for isotropic dipoles or lower atom densities [3, 4, 6–8, 12, 13, 35–37], since the interatomic interactions are predominantly long-range,  $F_{ji} \simeq \frac{e^{ik_e r_{ij}}}{ik_e r_{ij}}$ , and the contribution of the near-field terms  $\propto (k_e r_{ij})^{-2(3)}$  is small when  $k_e \langle r_{ij} \rangle \gg 1$ .

Increasing the atom number  $N$  and thereby the density in the same trapping volume accelerates the super-radiant decay, i.e. further increases  $\Gamma_S$ , and decelerates the sub-radiant decay, i.e. further decreases  $\Gamma_s$ , of the collective timed-Dicke state as seen in Fig. 3. On the other hand, increasing the atom number and proportionally the trapping volume to keep the atom density constant, we observe smaller modification of the super-radiant decay, consistent with Eq. (18). Finally, for a fixed atom density, changing only the width of the trap, but not its length, increases the sub-radiant fraction of the initial population (see the insets of Fig. 3), which indicates that the sub-radiant dynamics is mostly governed by the multiple scattering of the photons off the  $z$  axis, while the super-radiant emission happens mostly in the forward direction along  $z$ .

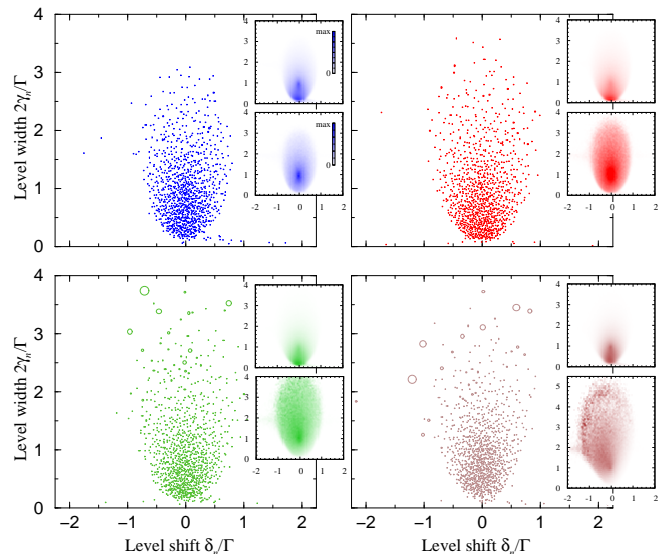


FIG. 4. Eigenvalues of the effective Hamiltonian (19) for  $N = 1000$  atoms in four different traps as in Fig. 2 (same color code, with the upper-left, upper-right, lower-left and lower-right panels corresponding to decreasing  $\sigma_{x,y}$  and increasing  $\sigma_z$ ). Main panels show the eigenvalues, as obtained for a single realization of the ensemble of atoms at random positions in the trapping volume; each eigenvalue  $\lambda_n = (\omega_e + \delta_n) - i\gamma_n$  is shown as a circle centered at the corresponding  $[\delta_n, \gamma_n]$  with the radius equal to the norm  $|\langle E_{\text{TD}} | \Psi_n \rangle|^2$  of the Franck-Condon overlap of the eigenstate  $|\Psi_n\rangle$  with the single-excitation state  $|E_{\text{TD}}\rangle$  of Eq. (16). The upper inset in each panel shows the spectrum of eigenvalues averaged over  $10^3$  random realizations of the ensemble, while the lower inset shows the same spectrum with each eigenvalue weighted by the corresponding FC factor (the shading is in arbitrary units, for best visibility).

## B. Single-excitation spectrum of the atoms

Equation (17) implies an effective non-Hermitian Hamiltonian for  $N$  interacting atoms:

$$H_{\text{eff}} = \sum_{j=1}^N \hbar \left( \omega_e - i\frac{\Gamma}{2} \right) |\tilde{e}_j\rangle \langle \tilde{e}_j| - i\frac{\Gamma}{2} \sum_{j=1}^N \sum_{j' \neq j}^N F_{jj'} e^{ik_e \cdot r_{j'j}} |\tilde{e}_j'\rangle \langle \tilde{e}_j|. \quad (19)$$

The solution of the eigenvalue problem  $H_{\text{eff}} |\Psi\rangle = \hbar\lambda |\Psi\rangle$  results in  $N$  generally non-orthogonal (right) eigenstates  $|\Psi_n\rangle$  with complex eigenvalues  $\lambda_n$ . The real part of each eigenvalue  $\text{Re}(\lambda_n) = \omega_e + \delta_n$  determines the level shift  $\delta_n$  of the corresponding eigenstate from the single-atom resonance  $\omega_e$ , while the imaginary part  $\text{Im}(\lambda_n) = -\gamma_n$  yields the level width or (half-)decay rate  $\gamma_n$  of the eigenstate.

Note that for a non-interacting system with  $F_{jj'} = 0 \forall j' \neq j$ , all  $N$  eigenstates would be degenerate,  $\lambda_n = \omega_e - i\Gamma/2$ , and we could construct one “bright” eigenstate  $|\Psi_B\rangle = |E_{\text{TD}}\rangle$  that corresponds to the timed-Dicke state of Eq. (16), while all the other eigenstates

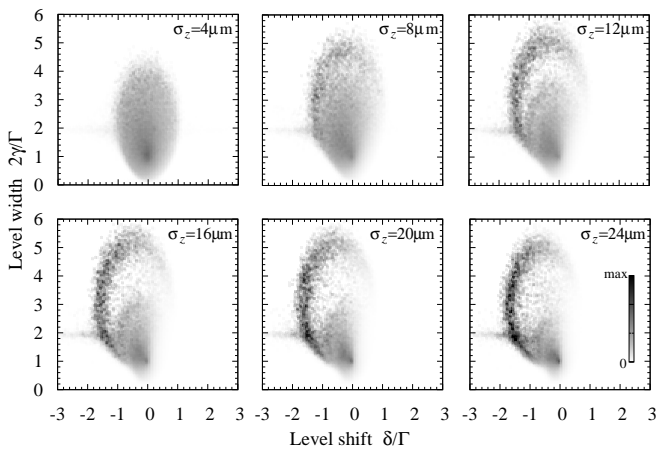


FIG. 5. Density of eigenvalues weighted by the corresponding FC factors  $|\langle E_{\text{TD}}|\Psi_n\rangle|^2$  averaged over  $10^3$  random realizations of the ensemble of  $N = 1000$  atoms in the elongated harmonic traps with lengths  $\sigma_z = 4, 8, \dots, 24 \mu\text{m}$  and widths  $\sigma_{x,y} = \sqrt{8/\sigma_z}$ , i.e., the same effective volume  $V_{\text{eff}} = (2\pi)^{3/2}\sigma_x\sigma_y\sigma_z = (2\pi)^{3/2}8\mu\text{m}^3$ , and mean interatomic separation  $\langle |\mathbf{r}_{ij}| \rangle = \sqrt[3]{V_{\text{eff}}/N} \simeq 0.5 \mu\text{m}$  as in Figs. 2 and 4.

would be “dark”,  $\langle E_{\text{TD}}|\Psi_{n \neq B}\rangle = 0$ , i.e., not accessible from either the ground or the storage state by a uniform laser field with wavevector  $\mathbf{k}_c$  (see below).

In Fig. 4 we show the spectrum of the effective Hamiltonian (19) for each of the four geometries of the trap with  $N = 1000$  atoms. Since the eigenstates  $|\Psi_n\rangle$  of the interacting system can be populated either from the ground state  $|G\rangle$  or from the collective storage state  $|S\rangle$  using a near-resonant laser with wavevector  $\mathbf{k}_c$ , we calculate the Franck-Condon (FC) overlap  $\langle E_{\text{TD}}|\Psi_n\rangle$  of each eigenstate with the timed-Dicke state of Eq. (16). We observe that the spectrum of the effective Hamiltonian has super-radiant,  $\gamma_n > \Gamma/2$ , and sub-radiant,  $\gamma_n < \Gamma/2$ , states, and most of the sub-radiant states have small level shifts  $|\delta_n| \lesssim \Gamma$ , while the super-radiant states have a broader spectrum of shifts from the atomic transition resonance  $\omega_e$ . For trap dimensions  $\sigma_{x,y} \sim \sigma_z$  the averaged spectrum, and the spectrum of eigenstates weighted by the FC factors, are approximately symmetric about the resonance,  $\delta = 0$ . But in the elongated trap  $\sigma_z \gg \sigma_{x,y}$  the super-radiant states with the largest FC factors tend to be shifted towards the lower frequencies  $\delta < 0$  (see the lower right panel of Fig. 4). This effect is even better pronounced for highly elongated traps, as shown in Fig. 5, and it is closely related to the collective shift of resonant light scattering by a one-dimensional atomic medium, due to constructive interference of the red-detuned light, as reported in [38].

The amplitude  $B_n(t)$  of an eigenstate  $|\Psi_n\rangle$  excited with probability  $|B_n(0)|^2$  at time  $t = 0$  evolves according to  $B_n(t) = B_n(0)e^{-i\lambda_n t}$ . Taking the Fourier transform  $\int_0^\infty dt B_n(t)e^{i\omega t}$ , we can then associate with each eigenstate having the decay rate  $\gamma_n$  and level shift  $\delta_n$  a Lorentzian emission/absorption line  $\frac{|B_n(0)|^2 \gamma_n^2}{(\Delta - \delta_n)^2 + \gamma_n^2}$

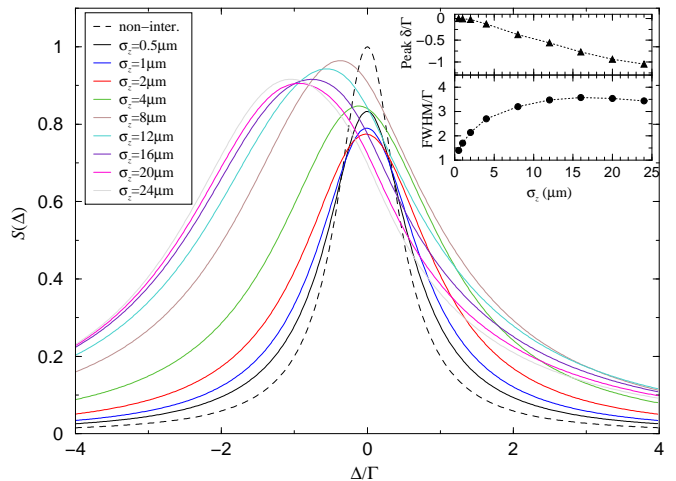


FIG. 6. Excitation spectrum  $S(\Delta)$  of Eq. (20) for  $N = 1000$  atoms in harmonic traps with different length  $\sigma_z$  and width  $\sigma_{x,y} = \sqrt{8/\sigma_z}$ , i.e., the same effective volume  $V_{\text{eff}} = (2\pi)^{3/2}\sigma_x\sigma_y\sigma_z = (2\pi)^{3/2}8\mu\text{m}^3$ . The spectrum is progressively broadened and shifted towards the negative detuning  $\Delta$  with increasing  $\sigma_z$ . For each geometry, the shown spectrum is averaged over  $10^3$  random realizations of the atomic ensemble. Insets show the peak position and full width at half maximum (FWHM) of each spectrum.

with  $\Delta = \omega - \omega_e$ . Since the excitation probability of each eigenstate from either the ground or the storage state via a laser with wavevector  $\mathbf{k}_c$  is proportional to  $|\langle E_{\text{TD}}|\Psi_n\rangle|^2$ , we can then define the excitation (absorption) spectrum of the systems as

$$S(\Delta) = \sum_{n=1}^N \frac{|\langle E_{\text{TD}}|\Psi_n\rangle|^2 \gamma_n^2}{(\Delta - \delta_n)^2 + \gamma_n^2}. \quad (20)$$

In Fig. 6 we plot  $S(\Delta)$  for various geometries of the atomic ensemble. With increasing length of the atomic ensemble, the excitation spectrum is progressively broadened and shifted towards the lower frequencies, i.e. negative detuning  $\Delta$ . This is expected from Fig. 5, which demonstrates that in the highly elongated atomic ensembles the eigenstates with the largest FC factors are super-radiant ( $\gamma > \Gamma/2$ ) and red-shifted ( $\delta < 0$ ) with respect to the single-atom resonance  $\omega_e$ . The red shift of the collective resonance in elongated atomic ensembles has been experimentally observed in Ref. [13].

### C. Angular emission profile

The (far) field emitted by the atoms, Eq. (9), in terms of the temporally and spatially slowly varying atomic amplitudes  $\tilde{b}_j = e^{-i\mathbf{k}_c \cdot \mathbf{r}_j} b_j$ , is given by

$$E_\sigma^{(\text{ff})}(\mathbf{r}, t) = (\hat{\mathbf{e}}_{\mathbf{r}, \sigma} \cdot \hat{\boldsymbol{\rho}}) \frac{\wp_{eg} k_e^2}{4\pi\epsilon_0} \frac{e^{i(\mathbf{k}_e \mathbf{r} - \omega_e t)}}{r} \times \sum_j \tilde{b}_j(t - r/c) e^{i(\mathbf{k}_c - \mathbf{k}_e) \cdot \mathbf{r}_j}, \quad (21)$$

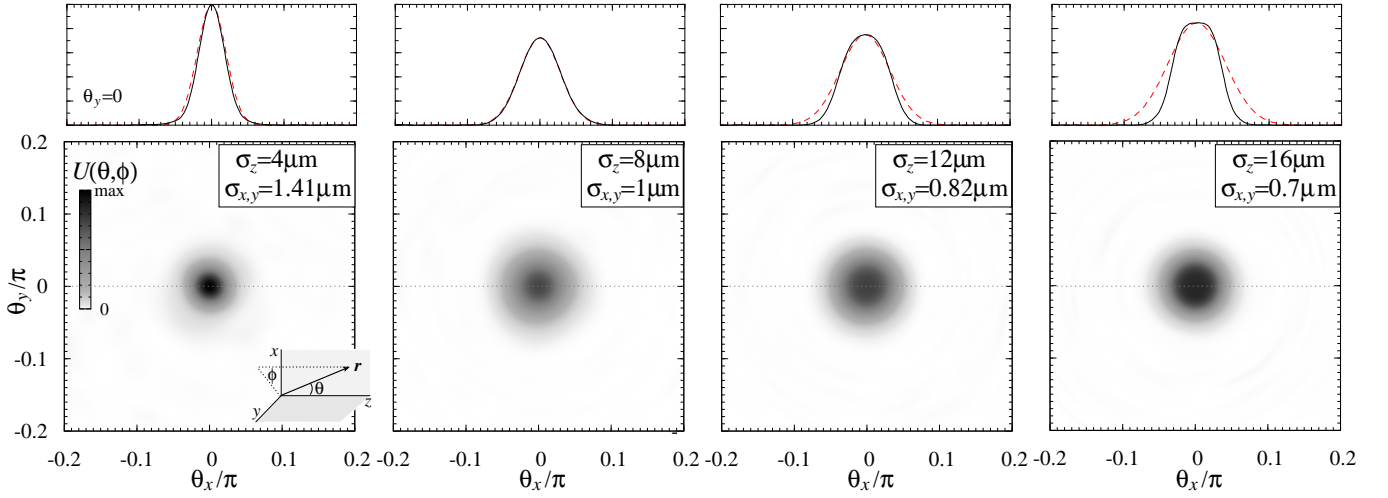


FIG. 7. Angular probability distribution  $U(\theta, \phi)$  of the photon emitted in the  $z$  direction, as a function of  $\theta_x = \theta \cos(\phi)$  and  $\theta_y = \theta \sin(\phi)$  with  $\theta$  the polar and  $\phi$  the azimuthal angles, for  $N = 1000$  atoms in elongated harmonic traps with the same effective volume  $V_{\text{eff}} = (2\pi)^{3/2} \sigma_x \sigma_y \sigma_z$  and different aspect ratios  $\sigma_{x,y}/\sigma_z$ . The black solid line in the upper inset of each density plot shows  $U(\theta_x, \theta_y = 0)$  while the red dashed line is the Gaussian of Eq. (22) with the corresponding width  $\Delta\theta = \frac{\sqrt{2}}{k_e \sigma_{x,y}}$ . Only the interval of  $|\theta| \leq 0.2\pi$  is shown as in the remaining solid angle only a weak noisy signal is present.

which clearly reveals the phase matching condition  $\mathbf{k}_e \simeq \mathbf{k}_c \parallel \hat{z}$  for constructive interference of photon emission. The intensity of the emitted radiation in the direction of  $\mathbf{r}$  is  $I_\sigma(\mathbf{r}, t) = \frac{\epsilon_0 c}{2} |E_\sigma(\mathbf{r}, t)|^2$ , while the total radiation (energy) collected by an ideal detector at position  $\mathbf{r}$  is  $U(\mathbf{r}) \delta s = \sum_{\sigma=1,2} \int_0^\infty dt I_\sigma(\mathbf{r}, t) \delta s$ , where  $\delta s$  is the surface element, or detector cross-section (pixel size), in the plane perpendicular to  $\mathbf{r}$ . From the discussion of Eq. (12), we expect that the angular distribution of the radiation emitted into the phase-matched direction  $z$  can be approximated by a Gaussian

$$U(\theta) \propto e^{-2\theta^2/\Delta\theta^2} \quad (22)$$

with the beam divergence  $\Delta\theta = \frac{\lambda_e}{\pi w_0} = \frac{\sqrt{2}}{k_e \sigma_\perp}$ . In Fig. 7 we show the angular probability distribution of  $U(\theta, \phi)$  which is highly peaked around  $\theta = 0$  due to cooperative photon emission into the phase-matched direction, while for larger angles  $\theta > \Delta\theta$  we observe a weak background noise due to spontaneous, uncorrelated photon emission by atoms at random positions. For large enough width  $\sigma_\perp$  of the atomic cloud, the emitted radiation profile is indeed Gaussian with the angular width  $\Delta\theta$ . But as the transverse width of the cloud becomes comparable to, or smaller than, the wavelength,  $\sigma_\perp \lesssim \lambda_e = 0.780 \mu\text{m}$ , the angular profile of the beam starts to strongly deviate from the Gaussian, i.e., it becomes narrower than the corresponding  $\Delta\theta$  and develops a “flat top”. We have checked that the narrowing effect is also present in the ensemble of non-interacting atoms, but the flattening of the top is effected by interatomic interactions. Thus, to maximize the collection of radiation from a highly elongated atomic cloud, one should engineer a lens with an appropriate non-circular curvature.

Our aim is to determine the probability of collecting the photon by an appropriate paraxial optics into the Gaussian mode

$$\phi_{k_e}(\mathbf{r}, t) = \frac{\zeta_{k_e} e^{-i k_e t}}{q_{k_e}^*(z)} \exp \left[ i k_e \left( z + \frac{x^2 + y^2}{2q_{k_e}^*(z)} \right) \right] \quad (23)$$

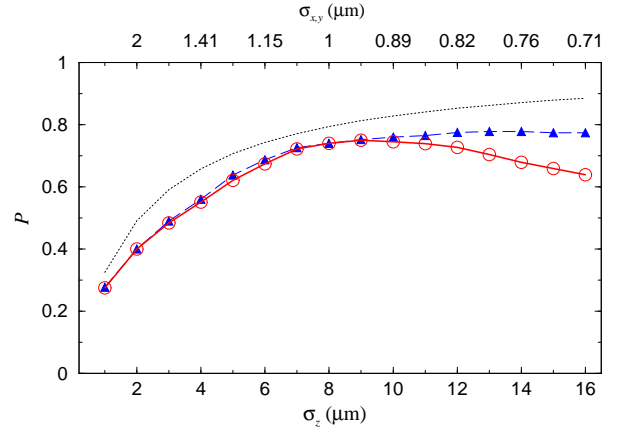


FIG. 8. Probability  $P$  of Eq. (24) for collecting the emitted photon into the Gaussian mode of waist  $w_0 = \sqrt{2}\sigma_{x,y}$  as a function of length  $\sigma_z$  (lower horizontal axis) or width  $\sigma_{x,y}$  (upper horizontal axis) of a cloud of  $N = 1000$  interacting atoms with fixed effective volume  $V_{\text{eff}} = (2\pi)^{3/2} \sigma_x \sigma_y \sigma_z = (2\pi)^{3/2} 8$  (red solid line with open circles). Also shown is the total probability of photon emission into the  $z$  direction within the solid angle  $\Omega_f = \pi(2\Delta\theta)^2$  (blue dashed line with filled triangles). For comparison, we also show the approximate analytic results of Eq. (15) for an ensemble of non-interacting atoms (black dotted line).

with the wavevector  $k_e$  and waist  $w_0 = \sqrt{2}\sigma_{x,y}$ . To this end, we calculate the overlap of the far field  $E_\sigma^{(\text{ff})}$  with  $\phi_{k_e}$  on a spherical surface with large radius  $r = \sqrt{x^2 + y^2 + z^2} \gg \sigma_{x,y,z}, \zeta_{k_e}$  integrating over the  $4\pi$  solid angle,  $\int_{4\pi} d\Omega_r [E_\sigma^{(\text{ff})}(\mathbf{r}, t) \phi_{k_e}^*(\mathbf{r}, t)]$ . The probability for the emitted photon to be collected into the Gaussian mode  $\phi_{k_e}^*(\mathbf{r})$  is then

$$P = \frac{\sum_{\sigma=1,2} \left| \int_{4\pi} d\Omega_r \int_0^\infty dt \frac{\epsilon_0 c}{2} [E_\sigma^{(\text{ff})}(\mathbf{r}, t) \phi_{k_e}^*(\mathbf{r}, t)] \right|^2}{\int d\Omega_r U(\mathbf{r}) \int d\Omega_r |\phi_{k_e}(\mathbf{r})|^2}. \quad (24)$$

In Fig. 8 we show  $P$  for various lengths  $\sigma_z$  and the corresponding widths  $\sigma_{x,y}$  or the atomic ensemble with the same effective volume and density. Note that the portion of the radiation emitted into the phase-matched direction  $z$  grows monotonically with increasing cloud length  $\sigma_z$ , although this growth nearly stops once the decreasing transverse width of the cloud becomes comparable to the wavelength,  $\sigma_{x,y} \lesssim \lambda_e = 0.780 \mu\text{m}$ . The probability  $P$  of the photon to be emitted into the appropriate Gaussian mode also grows initially with increasing  $\sigma_z$ , but it is peaked around  $\sigma_z \simeq 9 \mu\text{m}$  ( $\sigma_{x,y} \lesssim 1 \mu\text{m}$ ) and then decreases, since the spatial profile of the emitted radiation increasingly deviates from the Gaussian for narrower atom clouds [cf. upper insets in Fig. 7]. Note finally that the approximate analytic result of Eq. (15) for non-interacting atomic ensemble predicts larger emission probabilities into the Gaussian mode, but this result also does not take into account the narrowing of the emission profile for highly elongated atom clouds.

#### IV. THREE-LEVEL ATOMIC MEDIUM

In the previous section, we considered an ensemble of two-level atoms and assumed that initially the system is somehow prepared in the ideal timed-Dicke state with single collective excitation. But starting from the collective ground or storage state of the atomic ensemble, the preparation of the timed-Dicke state may be hindered by the strong interatomic interactions leading to spectral broadening and suppression of the transition to the collective excited states, as discussed in Sec. III B. We therefore consider now all three atomic levels, and assume that the initially populated collective storage state  $|S\rangle = \frac{1}{\sqrt{N}} \sum_{j=1}^N |s_j\rangle$  is coupled to the excited state by a laser with time-dependent Rabi frequency  $\Omega(t)$  and detuning  $\Delta_c$ , as shown in Fig. 1. The atomic amplitudes obey the equations

$$\partial_t c_j = i\Omega^* \tilde{b}_j e^{i\Delta_c t}, \quad (25a)$$

$$\partial_t \tilde{b}_j = i\Omega c_j e^{-i\Delta_c t} - \frac{1}{2}\Gamma \tilde{b}_j - \frac{1}{2}\Gamma \sum_{i \neq j} F_{ji} e^{i\mathbf{k}_c \cdot \mathbf{r}_{ij}} \tilde{b}_i. \quad (25b)$$

For non-interacting atoms [28],  $F_{ji} = 0$ , assuming a resonant laser  $\Delta_c = 0$  with sufficiently weak Rabi

frequency  $|\Omega| < \Gamma$ , we can set  $\partial_t \tilde{b}_j = 0$ , obtaining  $\tilde{b}_j \simeq i \frac{\Omega}{\Gamma/2} e^{i\mathbf{k}_c \cdot \mathbf{r}_j} c_j$ . Substituting this into Eq. (25a) and performing the integration, we have

$$c_j(t) \simeq c_j(0) \exp \left[ - \int_0^t dt' \frac{|\Omega(t')|^2}{\Gamma/2} \right], \quad (26a)$$

$$\tilde{b}_j(t) \simeq i \frac{\Omega(t)}{\Gamma/2} c_j(t), \quad (26b)$$

with the initial condition  $c_j(0) = 1/\sqrt{N} \forall j \in [1, N]$ . Using this solution in Eq. (9) or Eq. (21), we obtain

$$E_\sigma^{(\text{ff})}(\mathbf{r}, t) = i \frac{\wp_{eg} k_e^2}{4\pi\epsilon_0} \frac{\beta(t-r/c)}{\sqrt{N}} e^{-i\omega_e t} \mathcal{E}_\sigma(\mathbf{r}), \quad (27a)$$

$$\mathcal{E}_\sigma(\mathbf{r}) \equiv (\hat{\epsilon}_{\mathbf{r},\sigma} \cdot \hat{\wp}) \frac{e^{i\mathbf{k}_e \cdot \mathbf{r}}}{r} \sum_j e^{i(\mathbf{k}_e - \mathbf{k}_c) \cdot \mathbf{r}_j}, \quad (27b)$$

which, apart from the time dependence contained in  $\beta(t) \equiv \frac{\Omega(t)}{\Gamma/2} \exp \left[ - \int_0^t dt' \frac{|\Omega(t')|^2}{\Gamma/2} \right]$  and field polarization, is the same as Eqs. (10) with all the consequences discussed there. Detailed treatment of Raman conversion of collective atomic excitation in a non-interacting ensemble to a photon and its optimal collection via paraxial optics is presented in [28].

#### A. Dynamics of population transfer

For strongly interacting atoms, the above simple solution does not apply, and we resort to the numerical solutions of the atomic equations of motion (25). In Fig. 9 we show the dynamics of populations of the storage state  $p_S = \sum_j |c_j|^2$ , the excited state  $p_E = \sum_j |\tilde{b}_j|^2$  and the ground state  $p_G = 1 - p_S - p_E$  upon applying to the ensemble a coupling field with a smooth time-dependent Rabi frequency  $\Omega(t)$  and various detunings  $\Delta_c$  from the unperturbed atomic transition  $|s\rangle \rightarrow |e\rangle$ . It follows from the above discussion that the transition from the symmetric storage state  $|S\rangle$  to the collective excited state  $|E_{\text{TD}}\rangle$  driven by a uniform laser with wavevector  $\mathbf{k}_c \parallel \hat{z}$  is suppressed by either the small FC factors  $\langle E_{\text{TD}} | \Psi_n \rangle$  or large widths  $\gamma_n$  of the single excitation eigenstates  $|\Psi_n\rangle$ , which results in much slower population transfer as compared to the non-interacting atoms. Moreover, since the spectrum of the eigenstates  $|\Psi_n\rangle$  weighted by the corresponding FC factors is asymmetric and red-shifted from the atomic resonance frequency  $\omega_e$ , we observe stronger excitation, followed by decay, for negative detuning  $\Delta_c < 0$ . The inset in Fig. 9 shows the transfer probability to  $p_G$  at an intermediate time  $t = 2 \mu\text{s}$  as a function of  $\Delta_c$ , which is closely related to the excitation spectrum  $S(\Delta)$  of Fig. 6.

It is instructive to consider an effective three-level system with the ground state  $|G\rangle$ , the storage state  $|S\rangle$  and an excited state  $|E\rangle$  which is shifted from the single atom resonance by  $\delta_E$  and decays to the ground state with rate  $\Gamma_S > \Gamma$ . The initially populated storage state is coupled



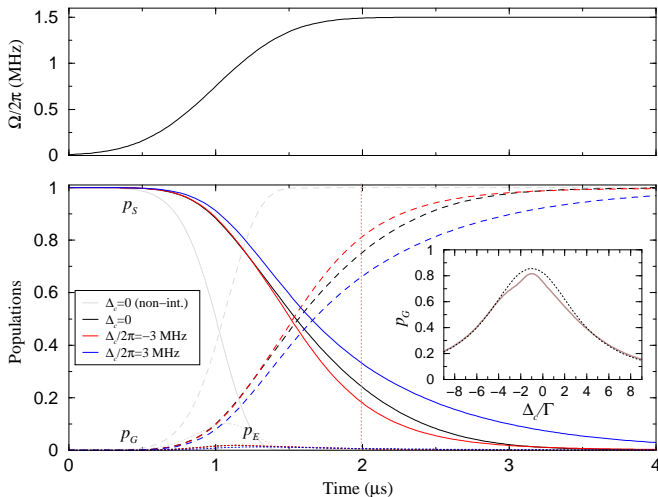


FIG. 9. Dynamics of population transfer of the atoms from the storage state to the excited state that decays to the ground state with the emission of a photon. The upper panel shows the time-dependence of the coupling field Rabi frequency  $\Omega(t) = \Omega_0 \frac{1}{2} [1 + \text{erf}(\frac{t-t_0}{\sqrt{2}\sigma_t})]$  with  $t_0 = 1 \mu\text{s}$  and  $\sigma_t = 0.4 \mu\text{s}$ . The lower panel shows the populations of the storage  $p_S$ , excited  $p_E$  and ground  $p_G$  states for three different detunings  $\Delta_c$  of the coupling field (with the detunings  $\Delta_c/2\pi = \pm 3$  MHz leading to slower/faster transfer compared to the  $\Delta_c = 0$  case), as obtained from averaging over  $10^2$  random realizations of the ensemble for  $N = 1000$  atoms in a harmonic trap with dimensions  $\sigma_z = 8 \mu\text{m}$  and  $\sigma_{x,y} = 1 \mu\text{m}$ . Also shown are the populations for an ensemble of non-interacting atoms under the same driving and decay conditions (light-gray curves). The inset shows the transfer probability to the ground state  $p_G$  at time  $t = 2 \mu\text{s}$  as a function of detunings  $\Delta_c$ , as obtained from a single realization of the random atomic ensemble (thick solid brown line), and as obtained from the approximate analytic solution of Eqs. (28) with parameters  $\Omega_{\text{eff}} = 0.92\Omega$ ,  $\delta_E = -1.0\Gamma$  and  $\Gamma_S = 6.0\Gamma$  (thin dotted black line); note that this value for  $\Gamma_S$  was obtained in Fig. 2 by fitting the decay curve for an initially excited atomic ensemble.

to the excited state  $|E\rangle$  with an effective Rabi frequency  $\Omega_{\text{eff}}$ . The amplitudes  $c$  and  $b$  of the storage and excited states obey the equations

$$\partial_t c = i\Omega_{\text{eff}}^* b e^{i(\Delta_c - \delta_E)t}, \quad (28a)$$

$$\partial_t b = i\Omega_{\text{eff}} c e^{-i(\Delta_c - \delta_E)t} - \frac{1}{2}\Gamma_S b, \quad (28b)$$

which have an approximate analytic solution similar to that of Eqs. (26), namely

$$c(t) \simeq c(0) \exp\left[-\int_0^t dt' \frac{|\Omega_{\text{eff}}(t')|^2}{\Gamma_S/2 - i(\Delta_c - \delta_E)}\right], \quad (29a)$$

$$b(t) \simeq i \frac{\Omega_{\text{eff}}(t) e^{-i(\Delta_c - \delta_E)t}}{\Gamma_S/2 - i(\Delta_c - \delta_E)} c(t), \quad (29b)$$

with  $c(0) = 1$ . The probability of population transfer to the ground state can then be approximated as  $p_G(t) = 1 - |c(t)|^2 - |b(t)|^2$ . In the inset in Fig. 9 we compare this analytic result with the exact numerical result and find

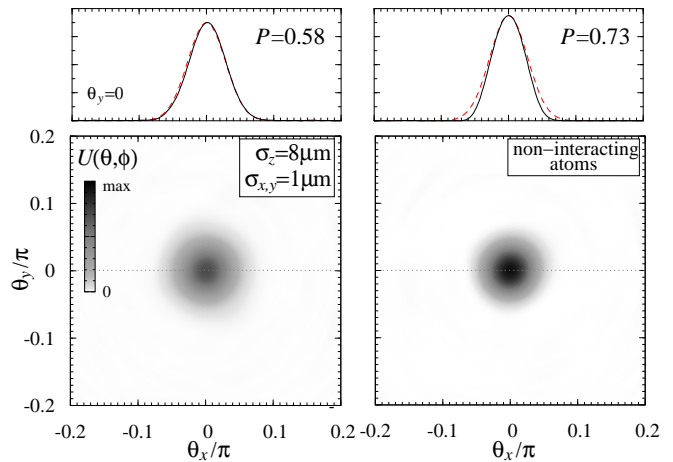


FIG. 10. Angular probability distribution  $U(\theta, \phi)$  of the photon emitted in the  $z$  direction for Raman excitation of the atomic cloud with all the parameters the same as in Fig. 9. The left panel shows  $U(\theta, \phi)$  vs.  $\theta_x = \theta \cos(\phi)$  and  $\theta_y = \theta \sin(\phi)$  as obtained for a single realization of the random atomic ensemble; For large integration times, the photon emission pattern is the same for different detunings  $\Delta_c$  of the coupling field, and the probability of cooperative emission into a Gaussian mode of waist  $w_0 = \sqrt{2}\sigma_{x,y}$  is  $P \simeq 0.583$ , with the remaining radiation incoherently scattered into all  $4\pi$  directions. The right panel shows  $U(\theta, \phi)$  for a non-interacting atomic ensemble under the otherwise identical conditions, leading to  $P \simeq 0.727$  [for comparison, the analytic result of Eq. (15) and Fig. 8 is  $P = 0.794$ ]. The black solid line in the upper inset of each density plot shows  $U(\theta_x, \theta_y = 0)$  while the red dashed line is the Gaussian of Eq. (22) with the corresponding width  $\Delta\theta = \frac{\sqrt{2}}{k_e \sigma_{x,y}}$ .

reasonable agreement for appropriate parameters  $\Omega_{\text{eff}}$ ,  $\delta_E$  and  $\Gamma_S$ .

## B. Radiation field

The angular distribution  $U(\theta, \phi)$  of the emitted radiation is shown in Fig. 10. We observe that for an interacting atomic ensemble the spatial profile of the radiation emitted in the phase-matched direction  $z$  closely matches a Gaussian mode of waist  $w_0 = \sqrt{2}\sigma_{x,y}$ . But the probability of cooperative emission into this Gaussian mode is rather small,  $P \simeq 0.58$ , since multiple photon scattering by the atoms results in large fraction  $1 - P \gtrsim 0.4$  of the radiation to be incoherently emitted into all  $4\pi$  directions. For comparison, for a non-interacting atomic ensemble we obtain a much larger  $P \simeq 0.73$ , even though the forward emitted radiation has somewhat narrower angular distribution than that of the expected Gaussian mode [for a slightly narrower Gaussian collection mode, we obtain  $P \simeq 0.77$  close to the theoretical result of Eq. (15) and Fig. 8]. Hence, dilute atomic ensembles with reduced multiple photon scattering seem to be better suited for achieving higher efficiency of photon collection into ap-

appropriate Gaussian modes [28].

Remarkably, even though the dynamics of population transfer between the collective atomic states depends on the detuning  $\Delta_c$  of the coupling field [cf. Fig. 9], for large integration times, when the population of the symmetric storage state of the atomic ensemble is completely depleted,  $p_S = 0$  and  $p_G \simeq 1$ , we obtain the same emission pattern  $U(\theta, \phi)$  and photon collection probability  $P \simeq 0.58$  of the interacting atomic ensemble for any detuning  $\Delta_c$ . Thus the atomic ensemble indeed behaves as an effective three-level medium with a single broad intermediate excited state [cf. inset in Fig. 9], rather than as a collection of single-excitation states  $|\Psi_n\rangle$  with different widths and coupling strengths.

## V. CONCLUSIONS

A topic of great interest of current research is the interaction of light with regular arrays of strongly (dipole-dipole) interacting atoms [39–45]. Such systems possess cooperative resonances corresponding to super- and sub-radiant optical modes and can serve as, e.g., perfect optical mirrors [39, 42, 44, 45] or tailored, highly-efficient photon emitters into the desired spatial modes [41, 43]. These unique properties, however, critically depend on the periodic, defect-free spatial arrangement of single atoms in lattices with subwavelength spacing.

Here, we have considered a high-density regime of random atomic ensembles with the subwavelength mean interatomic distance. This system permits a much smaller degree of control of the super- and sub-radiance and spatial emission pattern of the radiation, as compared to the perfectly periodic 1D, 2D or 3D arrays of atoms. Yet, the random atomic ensembles are much easier to real-

ize experimentally in various trapping geometries, which still allow a certain amount of control of their optical properties, as we have shown above. In particular, we have found that the phase-matched, super-radiant emission of radiation is strongly enhanced in elongated atomic ensembles, while multiple scattering of photons off the phase-matching direction is mainly responsible for the sub-radiant emission. It would be interesting to investigate how the super- and sub-radiant collective modes can be selectively suppressed or converted on demand into each other, and how to control and further enhance the directionality of the photon emission using, e.g., spatial and/or temporal modulation of the amplitudes and phases of the atoms in extended traps, which can be accomplished by spatially varying electric or magnetic fields or ac Stark shifts induced by off-resonant lasers. Finally, studying multiple excitations in strongly-interacting but random atomic ensembles beyond the linear optical regime would be an interesting and important problem to tackle via development of effective analytic and efficient numerical tools.

## ACKNOWLEDGMENTS

We thank rpad Kurko, Peter Domokos, Thomas Bekkegaard, and Jozsef Fortagh for useful discussions. We acknowledge support by the US ARL-CDQI program through cooperative agreement W911NF-15-2-0061. D.P. was supported by the EU QuantERA Project PACE-IN (GSRT grant No. T11EPA4-00015) and by the Alexander von Humboldt Foundation in the framework of the Research Group Linkage Programme. K.M. was supported by the Carlsberg Foundation through the Semper Ardens Research Project QCooLEU and by the Danish National Research Foundation Centre of Excellence for Complex Quantum Systems.

- 
- [1] R. H. Dicke, *Coherence in Spontaneous Radiation Processes*, Phys. Rev. **93**, 99 (1954).
  - [2] M. O. Scully, E. S. Fry, C. H. R. Ooi, and K. Wodkiewicz, *Directed Spontaneous Emission from an Extended Ensemble of  $N$  Atoms: Timing Is Everything* Phys. Rev. Lett. **96**, 010501 (2006).
  - [3] I. E. Mazets and G. Kurizki, *Multiatom cooperative emission following single-photon absorption: Dicke-state dynamics*, J. Phys. B **40**, F-105 (2007).
  - [4] A. A. Svidzinsky, J.-T. Chang, and M. O. Scully, *Dynamical Evolution of Correlated Spontaneous Emission of a Single Photon from a Uniformly Excited Cloud of  $N$  Atoms*, Phys. Rev. Lett. **100**, 160504 (2008).
  - [5] T. Bienaime, M. Petruzzo, D. Bigerni, N. Piovella, R. Kaiser, *Atom and photon measurement in cooperative scattering by cold atoms*, J. Mod. Phys. **58**, 1942 (2011).
  - [6] A. Svidzinsky and J.-T. Chang, *Cooperative spontaneous emission as a many-body eigenvalue problem*, Phys. Rev. A **77**, 043833 (2008).
  - [7] A. A. Svidzinsky, J.-T. Chang, and M. O. Scully *Cooperative spontaneous emission of  $N$  atoms: Many-body eigenstates, the effect of virtual Lamb shift processes, and analogy with radiation of  $N$  classical oscillators*, Phys. Rev. A **81**, 053821 (2010).
  - [8] T. Bienaime, N. Piovella, and R. Kaiser, *Controlled Dicke Subradiance from a Large Cloud of Two-Level Systems*, Phys. Rev. Lett. **108**, 123602 (2012).
  - [9] W. Guerin, M. O. Araujo, and R. Kaiser *Subradiance in a Large Cloud of Cold Atoms*, Phys. Rev. Lett. **116**, 083601 (2016).
  - [10] R. A. de Oliveira, M. S. Mendes, W. S. Martins, P. L. Saldanha, J. W. R. Tabosa, and D. Felinto, *Single-photon superradiance in cold atoms*, Phys. Rev. A **90**, 023848 (2014).
  - [11] L. Ortiz-Gutierrez, L. F. Munoz-Martinez, D. F. Barros, J. E. O. Morales, R. S. N. Moreira, N. D. Alves, A. F. G. Tieco, P. L. Saldanha, and D. Felinto, *Experimental Fock-State Superradiance*, Phys. Rev. Lett. **120**, 083603 (2018).
  - [12] M. O. Araujo, I. Kreic, R. Kaiser, and W. Guerin, *Superradiance in a Large and Dilute Cloud of Cold Atoms in the Linear-Optics Regime*, Phys. Rev. Lett. **117**, 073002 (2017).

- (2016).
- [13] S. J. Roof, K. J. Kemp, M. D. Havey, and I. M. Sokolov, *Observation of Single-Photon Superradiance and the Cooperative Lamb Shift in an Extended Sample of Cold Atoms*, Phys. Rev. Lett. **117**, 073003 (2016).
- [14] W. Guerin, T. S. do Espirito Santo, P. Weiss, A. Cipris, J. Schachenmayer, R. Kaiser, and R. Bachelard, *Collective Multimode Vacuum Rabi Splitting*, Phys. Rev. Lett. **123**, 243401 (2019).
- [15] R. H. Lehmburg, *Radiation from an N-Atom System*, Phys. Rev. A **2**, 883 (1970); **2**, 889 (1970).
- [16] D.P. Craig and T. Thirunamachandran, *Molecular Quantum Electrodynamics* (Academic Press, London, 1984).
- [17] S. D. Jenkins, J. Ruostekoski, J. Javanainen, S. Jennewein, R. Bourgain, J. Pellegrino, Y. R. P. Sortais, and A. Browaeys, *Collective resonance fluorescence in small and dense atom clouds: Comparison between theory and experiment* Phys. Rev. A **94**, 023842 (2016).
- [18] L. Corman, J. L. Ville, R. Saint-Jalm, M. Aidelsburger, T. Bienaime, S. Nascimbene, J. Dalibard, and J. Beugnon, *Transmission of near-resonant light through a dense slab of cold atoms*, Phys. Rev. A **96**, 053629 (2017).
- [19] M. Fleischhauer, A. Imamoglu, and J. P. Marangos, *Electromagnetically induced transparency: Optics in coherent media*, Rev. Mod. Phys. **77**, 633 (2005).
- [20] K. Hammerer, A. S. Sørensen, and E. S. Polzik, *Quantum interface between light and atomic ensembles*, Rev. Mod. Phys. **82**, 1041 (2010).
- [21] N. Sangouard, C. Simon, H. de Riedmatten, and N. Gisin, *Quantum repeaters based on atomic ensembles and linear optics*, Rev. Mod. Phys. **83**, 33 (2011).
- [22] G. Kurizki, P. Bertet, Y. Kubo, K. Mølmer, D. Petrosyan, P. Rabl, J. Schmiedmayer, *Quantum technologies with hybrid systems*, PNAS **112**, 3866 (2015).
- [23] D. Petrosyan, K. Mølmer, J. Fortágh, M. Saffman, *Microwave to optical conversion with atoms on a superconducting chip*, New J. Phys. **21**, 073033 (2019).
- [24] J. P. Covey, A. Sipahigil, M. Saffman, *Microwave-to-optical conversion via four-wave mixing in a cold ytterbium ensemble*, Phys. Rev. A **100**, 012307 (2019).
- [25] N. Lauk, N. Sinclair, S. Barzanjeh, J. P. Covey, M. Saffman, M. Spiropulu, and C. Simon, *Perspectives on quantum transduction*, Quantum Sci. Technol. **5**, 020501 (2020).
- [26] H.J. Kimble, *The quantum internet*, Nature **453**, 1023 (2008).
- [27] J. L. O’Brien, A. Furusawa and J. Vuckovic, *Photonic quantum technologies*, Nature Photon. **3**, 687 (2009).
- [28] A. Kurko, P. Domokos, A. Vukics, T. Bækkegaard, N.T. Zinner, J. Fortágh, D. Petrosyan, *Optimal collection of radiation emitted by a trapped atomic ensemble*, arXiv:2011.07094 [quant-ph].
- [29] We may assume a closed transition between the states  $|g\rangle = |5S_{1/2}, F = 2, m_F = 2\rangle$  and  $|e\rangle = |5P_{3/2}, F = 3, m_F = 3\rangle$  of  $^{87}\text{Rb}$ , while the storage state  $|s\rangle = |5S_{1/2}, F = 1, m_F = 1\rangle$  is coupled to  $|e\rangle$  via a two-photon (microwave mediated) transition with the effective Rabi frequency  $\Omega$ . Alternatively, the storage state  $|s\rangle$  can also be a long-lived  $nS$  or  $nD$  Rydberg state [23, 30–32].
- [30] M. Saffman and T. G. Walker, *Entangling single- and N-atom qubits for fast quantum state detection and transmission*, Phys. Rev. A **72**, 042302 (2005).
- [31] D. Petrosyan, K. Mølmer, *Deterministic free-space source of single photons using Rydberg atoms* Phys. Rev. Lett. **121**, 123605 (2018).
- [32] Y. Miroshnychenko, U. V. Poulsen, and K. Mølmer, *Directional emission of single photons from small atomic samples* Phys. Rev. A **87**, 023821 (2013).
- [33] M. O. Scully and M. S. Zubairy, *Quantum Optics* (Cambridge University Press, Cambridge, 1997).
- [34] P. Lambropoulos and D. Petrosyan, *Fundamentals of Quantum Optics and Quantum Information* (Springer, Berlin, 2007)
- [35] A. S. Kuraptsev, I. M. Sokolov, and M. D. Havey, *Angular distribution of single-photon superradiance in a dilute and cold atomic ensemble*, Phys. Rev. A **96**, 023830 (2017).
- [36] M. O. Araujo, W. Guerin, and R. Kaiser, *Decay dynamics in the coupled-dipole model*, J. Mod. Opt. **65**, 1345 (2018).
- [37] C. E. Maximo, R. Bachelard, F. E. A. dos Santos, and C. J. Villas-Boas, *Cooperative spontaneous emission via a renormalization approach: Classical versus semiclassical effects*, Phys. Rev. A **101**, 023829 (2020).
- [38] A. Glicenstein, G. Ferioli, N. Šibalić, L. Brossard, I. Ferrier-Barbut, and A. Browaeys, *Collective Shift in Resonant Light Scattering by a One-Dimensional Atomic Chain*, Phys. Rev. Lett. **124**, 253602 (2020).
- [39] R. J. Bettles, S. A. Gardiner, and C. S. Adams, *Enhanced Optical Cross Section via Collective Coupling of Atomic Dipoles in a 2D Array*, Phys. Rev. Lett. **116**, 103602 (2016).
- [40] G. Facchinetti, S. D. Jenkins, and J. Ruostekoski, *Storing Light with Subradiant Correlations in Arrays of Atoms*, Phys. Rev. Lett. **117**, 243601 (2016).
- [41] A. Asenjo-Garcia, M. Moreno-Cardoner, A. Albrecht, H. J. Kimble, and D. E. Chang, *Exponential Improvement in Photon Storage Fidelities Using Subradiance and “Selective Radiance” in Atomic Arrays*, Phys. Rev. X **7**, 031024 (2017).
- [42] E. Shahmoon, D. S. Wild, M. D. Lukin, and S. F. Yelin, *Cooperative Resonances in Light Scattering from Two-Dimensional Atomic Arrays*, Phys. Rev. Lett. **118**, 113601 (2017).
- [43] A. Grankin, P. O. Guimond, D. V. Vasilyev, B. Vermaersch, and P. Zoller, *Free-space photonic quantum link and chiral quantum optics*, Phys. Rev. A **98**, 043825 (2018).
- [44] P.-O. Guimond, A. Grankin, D. V. Vasilyev, B. Vermaersch, and P. Zoller, *Subradiant Bell States in Distant Atomic Arrays*, Phys. Rev. Lett. **122**, 093601 (2019).
- [45] J. Rui, D. Wei, A. Rubio-Abadal, S. Hollerith, J. Zeiher, D. M. Stamper-Kurn, C. Gross, and I. Bloch, *A subradiant optical mirror formed by a single structured atomic layer*, Nature **583**, 369 (2020).